Eur. Phys. J. D **17**, 93–98 (2001)

THE EUROPEAN PHYSICAL JOURNAL D

EDP Sciences

Numerical simulation of spatial fluctuations in parametric image amplification

E. Lantz[a] and F. Devaux

Laboratoire d'Optique P.M. Duffieux[b], Université de Franche-Comté, 25030 Besançon Cedex, France

Received 12 March 2001

Abstract. We study the properties of the spatial fluctuations in the far-field parametric fluorescence output of a type 1 degenerate traveling-wave parametric amplifier. Results of a semi-classical simulation are compared with experiments in a LBO crystal. This simulation is then used to predict amplified images of a continuous background, in a phase-sensitive as well as in a phase-insensitive configuration.

PACS. 42.50.-p Quantum optics – 42.50.Lc Quantum fluctuations, quantum noise, and quantum jumps – 42.65.Yj Optical parametric oscillators and amplifiers

1 Introduction

Reducing quantum fluctuations of light in imaging systems has recently attracted a considerable interest. Many phenomena that are now well-known in the time-domain have been shown to have their counterpart in the spatial domain, like noiseless image amplification [1–3], image entanglement [4,5] or generation of multimode squeezing [6]. However, the reduction of quantum fluctuations is often shown, even in these studies, still in the time domain. For example, the experiment in the group of Kumar [1] shows that a phase-sensitive scheme allows the signal-to-noise-ratio to be unmodified by the parametric amplification over an entire image, where the noise is recorded at a frequency of 27 MHz by a photodiode with a detection area smaller than the resolution cell. Because the photodiode scans the image, this result proves that phase-sensitive amplification improves the regularity in time of the distribution of photons for each point of the image but does not directly show a regularity in space because only fluctuations in the time-domain at a specific frequency are recorded. However, fluctuations in quantum mechanics are described by ensemble averages, that are often estimated by time averages if the signal is stationary in time, but which can be also estimated by spatial averages if the signal is stationary in space on a sufficiently large area. This point of view has been developed in theoretical studies either by computing the spatial frequency spectrum of quantum fluctuations [6] or by studying spatial correlations [7]. However, purely spatial quantum fluctuations have not yet been experimentally evidenced. These spatial fluctuations will limit the ultimate precision in spatial measurements, like for example measurements of displacements [8]. In our recent work on spontaneous down-conversion in a LBO crystal [9], we showed that spatial fluctuations in the far-field image exhibited strong correlations between symmetrical areas. However, the experimental set-up did not allow us to conclude on their quantum character. This paper presents numerical simulations of spatial fluctuations resulting from the amplification of quantum noise, at the same semi-classical level. In particular the paper does not aim at demonstrating purely quantum effects, like *e.g.* sub-Poissonnian statistics of differences [4]. It is organized as follows. We briefly review in Section 2 the experimental results reported in [9], compare them in Section 3 to a numerical semi-classical model and in Section 4 we simulate with this model the detected images resulting from the amplification of a continuous background.

2 Experiment

The experimental set-up is illustrated in Figure 1. The pump pulses of 40 ps duration, with a time-bandwidth product close to 1, are generated by a frequency-doubled Q-switched mode-locked Nd:YAG laser at a repetition rate of 10 Hz and at a wavelength of 532 nm. The beam has an elliptical transverse section with $\Delta x = 0.44$ mm, $\Delta y = 0.12$ mm and is vertically polarized in the XY-plane of a 15 mm long LBO crystal whose lateral dimensions are 4×4 mm^2. A beam splitter BS before the crystal permits the measurement of the pump pulse energy with an energymeter. The transmitted part of the collimated pump beam illuminates the input face of the crystal and a dichroic mirror separates it from the fluorescence signal after the crystal. The spatial frequency spectrum of the parametric fluorescence is imaged in the image focal plane of the lens L (Fourier plane) by a single-shot CCD

[a] e-mail: elantz@univ-fcomte.fr
[b] UMR 6603 du CNRS

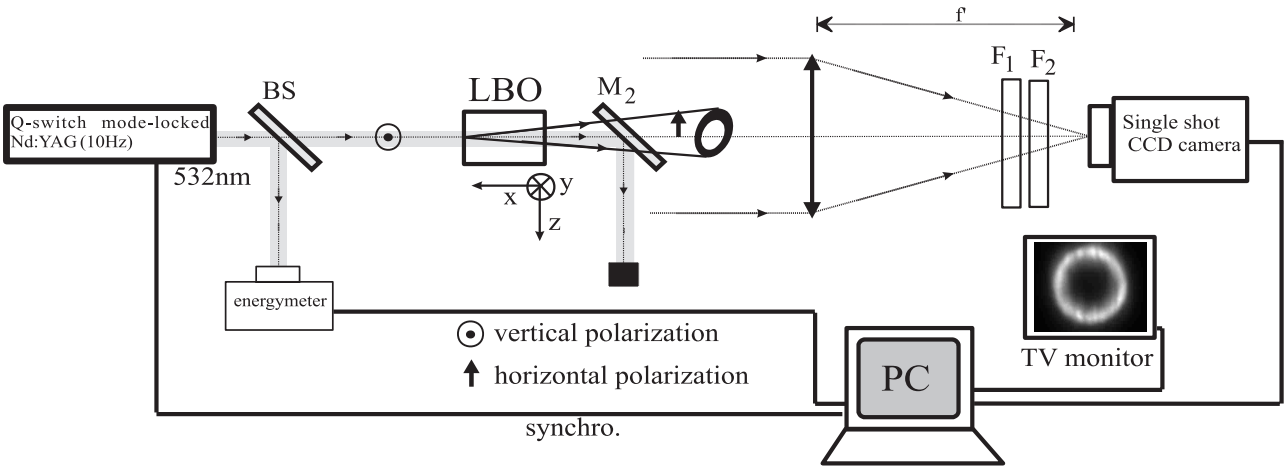

Fig. 1. Experimental set-up used to study the spatial properties of parametric fluorescence.

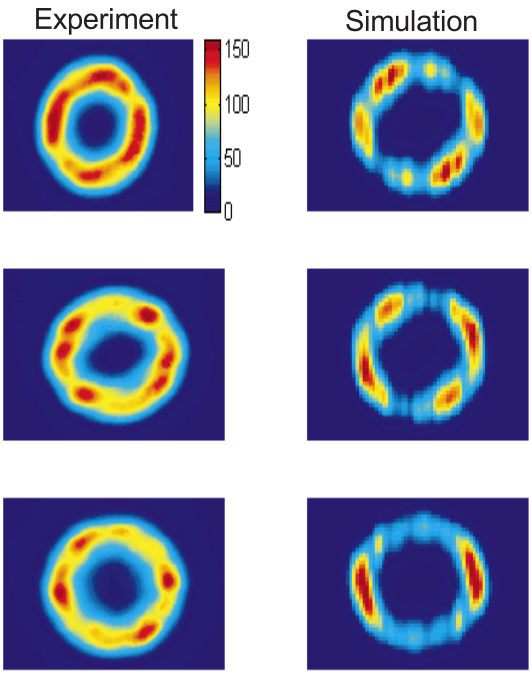

Fig. 2. Sequence of three spatial frequency spectra obtained with the same phase matching conditions and approximately the same pump energy. Each spectrum corresponds to one laser shot.The spectra in (a) are experimental, while those in (b) are obtained by numerical simulation.

camera. A RG5 filter F1 and a narrow band ($\Delta\lambda = 5$ nm) interference filter F2, centered around the degenerate frequency ($\lambda = 1064$ nm), are placed in front of the CCD camera in order to limit the number of detected temporal modes around degeneracy. The CCD camera and the energymeter are monitored by a computer synchronized with the laser. Hence, the far field distribution of the fluorescence signal is measured shot to shot with respect to the pump pulse energy.

Figure 2a represents a sequence of three far-field images obtained for the same phase matching conditions, corresponding to the amplification of a ring, and with approximately the same pump pulse energy. The spatial fluctuations vary from one shot to another. However, spatial correlation between pairs of spatial modes that are symmetrically distributed around the pump beam direction is clearly exhibited [10]. Figure 3a shows the experimental autocorrelation functions along a circular profile corresponding to perfect phase matching at degeneracy. This circular profile is experimentally determined as that where the detected mean intensity is maximum. The most prominent feature of these functions is the almost perfect correlation for an angle of 180°. It means that fluctuations of areas that are opposite to each other with respect to the pump direction are strongly correlated, because of the twin-photon emission at degeneracy. Though strong, the correlation is not perfect because of the classical noise. Furthermore, the autocorrelation function is computed in the classical signal processing way, that ensures a maximum of the autocorrelation at 0°. This function cannot be directly compared with the quantum correlation, that measures the joint probability of the detection of a pair of photons at two points. It has been proved in [7] that this quantum correlation is higher at 180° than at 0°. A direct experimental measurement of the quantum correlation function would require a single photon sensitivity that was not available in the described experiment. We compare in the next section the size and the contrast of the fluctuations obtained in this experiment with a semi-classical simulation.

3 Numerical simulation

The semi-classical model of spontaneous down-conversion assumes an input quantum noise of one photon per spatio-temporal mode. Figure 2b shows images of far-field parametric fluorescence obtained by a computation using the following procedure:

– at the input of the crystal, the field is simulated by a white noise, with a random phase and a Gaussian

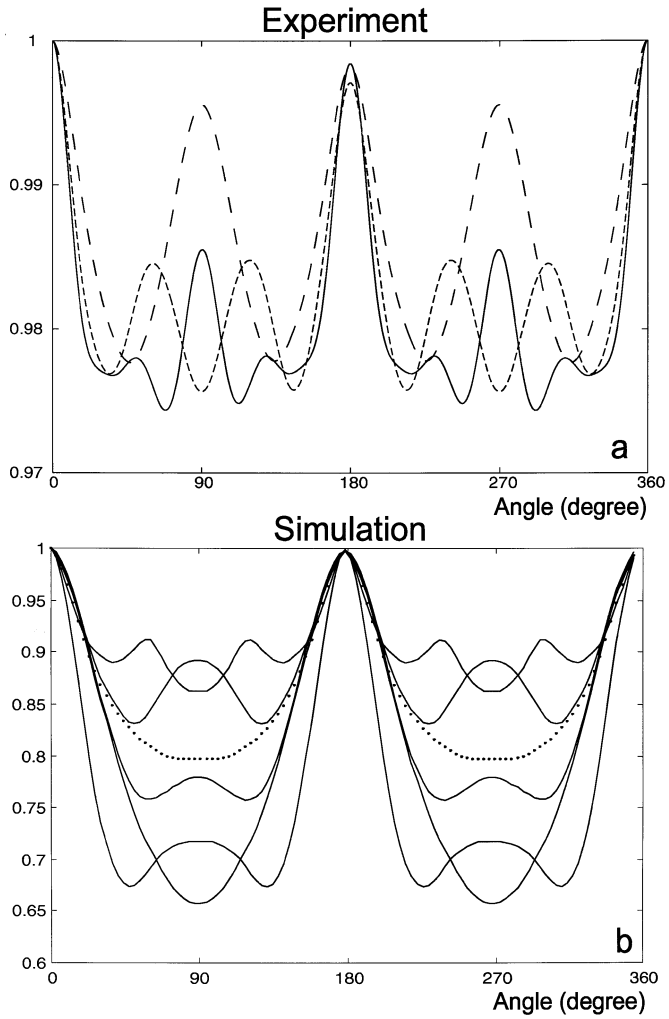

Fig. 3. (a) Autocorrelation functions of the 1-D intensity profiles obtained on the best phase matching circles (corresponding to the maximum detected intensity) for the spectra of Figure 2a. The continuous background has been removed. (b) Solid lines: five autocorrelation functions obtained from simulated spectra; dotted line: mean of ten autocorrelation functions.

distributed amplitude that corresponds to a mean energy for each sample equal to that of one photon. The only constraint for the sampling frequency is to be greater than twice the spatial frequency that corresponds to the external radius of the phase matching ring;
- the pump field, supposed undepleted by the fluorescence, is determined from its experimental image at the output face of the crystal (near-field) and from measurements of its total energy and duration. This field is used as the phase reference;
- the signal field is propagated in Fourier space, taking into account the pump-signal phase mismatch for colinear propagation, and coherently amplified in the direct space by using the classical coupled equations of parametric amplification. Note that, because of complete degeneracy, these equations link the pump, the signal and the complex conjugate of the signal. The idler and the signal waves are completely indistinguishable;
- the simulation is repeated for each temporal mode, whose duration (0.8 ps) is proportional to the reciprocal of the interference filter bandwidth. This duration corresponds to a time interval in the pump Gaussian pulse where the pump amplitude can be considered as constant. To simulate the integration by the CCD camera, the far-field images of all temporal modes are incoherently added.

A direct quantitative comparison between the experimental and the simulated images is not possible, because of the random character of these images. However, the qualitative similarity is evident. In particular, the mean size of the fluctuations is similar and can be estimated as the reciprocal area in the spatial frequency domain of the fluorescence beam at the output of the crystal [9]. Note that the section of the fluorescence beam is much smaller than that of the pump beam, because of the high gain (about 60 dB) and of the Gaussian spatial profile of the pump beam. On the other hand, the contrast in the simulated images is somewhat higher than in the experimental ones. The explanation could reside in either the experimental conditions (a slight defocusing could be invoked) or an under-estimation of the number of temporal modes. The contrast in the simulated images for a single temporal mode is unity, in good agreement with theory [3,4].

The last important point is the perfect correlation between opposite pixels in the simulated images. Because of the classical nature of the simulation, where fields rather than photons are propagated, this correlation is classical and the sub-Poissonnian statistics on the difference between opposite pixels [4,7] cannot be evidenced. Figure 3b shows five autocorrelation functions on the circle of best phase matching of the simulated images. One of these functions exhibits two secondary peaks at 90°, like two experimental autocorrelation functions. However, these peaks are not present in all images, experimental as well as simulated, and their random existence can be attributed to the great size of the fluctuations. To confirm that point, the mean of ten autocorrelation functions, also shown in Figure 3b, exhibits only peaks at 0° and 180°, as expected.

4 Simulation of the amplification of a continuous background

When the signal and the idler channels are both excited in type 1 or type 2 amplification, the amplification gain depends on the input relative phase of the interacting waves. Such a phase sensitive amplifier (PSA) can be used to amplify beams limited by the shot noise without degrading the signal-to-noise ratio, while a phase-insensitive amplifier (PIA) adds 3 dB of noise [11,12]. A PSA can also be used to noiselessly amplify an image [1–3]. We use in the following the numerical simulation described above to obtain near-field images of the amplification of a continuous background, with a unity quantum efficiency of the

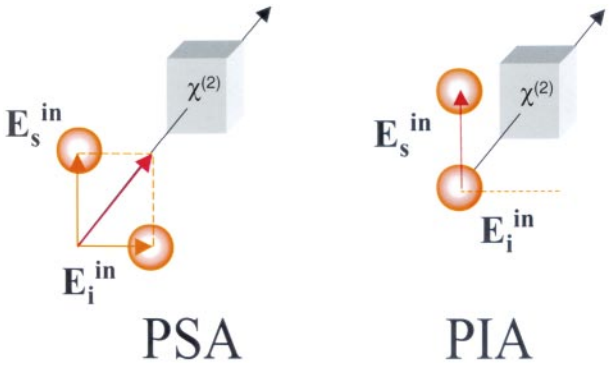

Fig. 4. PIA: coherent signal with Gaussian noise on the signal channel and 1/2 photon of noise/pixel on the idler channel. PSA: projection of the classical field onto the two channels +1/2 photon of noise/pixel.

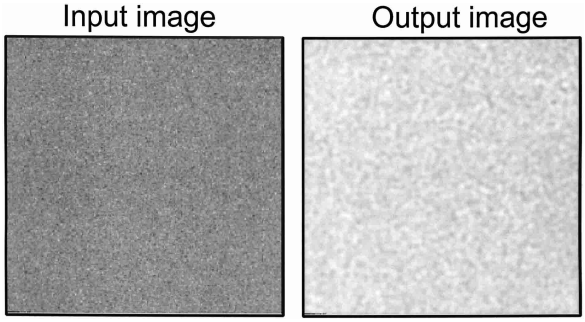

Fig. 5. Result of the numerical simulation for PSA: spatial inhomogeneities are wider in the output image than in the input image.

detector. These near-field images correspond to our experimental scheme of parametric image amplification [13], also used in reference [1], where the object is imaged in the crystal and then on a CCD Camera. On the other hand, the theory developed in references [3,4] considers a crystal in the Fourier plane of the imaging system.

The input image, a plane wave with a mean intensity constant in the transverse plane, is amplified at degeneracy by a type 2 parametric interaction in a 2 cm long KTP crystal with a 7×7 mm^2 section. The shot noise is simulated by adding to the classical field a random field with a Gaussian distribution corresponding to a mean amplitude of 1/2 photon per pixel in the input image for both polarisations [11]. As shown in Figure 4, PIA occurs when a coherent signal is amplified on one polarisation, while the idler channel, corresponding to the other polarisation, is excited by half a photon of noise per pixel. PSA is obtained when the classical field is polarised at 45 degrees with respect to the signal and idler axes. After projection of this classical field onto these axes, the random field is independently added on each axis.

Figure 5 shows results of the numerical simulation. The input image has 256×256 pixels, a mean number of 50 photons/pixel and the maximum parametric gain in a PSA configuration is 17 dB. In order to directly evaluate the regularity in space of the intensity, the signal-to-noise ratio is estimated by a statistical average on the pixels of a single image by [12]:

$$\mathrm{SNR} = \frac{\langle N \rangle^2}{\langle N - \langle N \rangle \rangle^2} \cdot \tag{1}$$

In (1), N is the number of photons on one pixel. Because the simulation involves fields rather than photons, this number is not necessarily an integer. Surprisingly, the noise figure NF, defined as the ratio between the input and the output signal-to-noise ratio, is smaller than one, NF(PSA) = 0.14, that corresponds to an apparent improvement of the signal-to-noise ratio. Actually, phase matching acts as a low pass-filter that rejects the high frequency noise, resulting in inhomogeneities in the amplified image that have a greater spatial size than the spatial fluctuations in the input image (see Fig. 5). As the SNR must be defined in the bandwidth of the amplifier, the size of the pixels must be greater than the size of the resolution cell in the amplified image. From an other, but equivalent, point of view [3], using too small pixels can be seen as introducing detection losses that deteriorate the SNR that would result of the detection of the input Poissonnian image, while the amplified image is less sensitive to detection losses because of its super-Poissonnian statistics. As expected, taking in account pixels greater than the resolution cell results in a NF(PSA) close to 1 and a NF(PIA) close to 2: Figure 6a shows that such pixels are obtained by binning at least 8×8 CCD pixels, while the size(FWHM) of the resolution cell is approximately 4×4 pixels. This size has been estimated on the amplified image of a delta-like object, *i.e.* an object with a single pixel where the intensity is non zero. However, the calculated noise figure remains somewhat smaller than the actual one, leading to results eventually slightly below the unity in Figures 6b–6d, because binning does not correspond to a perfect low-pass filter. Figure 6b shows the variation of the NF with respect to the input relative phase, for sufficiently great pixels. The numerical simulation is fitted with the curve of the theoretical NF(PSA) for one degenerate mode at perfect phase-matching given by:

see equation (2) below

where N_{in} is the number of photons per mode at the input, φ is the phase of the input signal with respect to the amplified quadrature and r is the gain factor. Equation (2) is valid for an image because only low spatial frequencies are involved in the amplification of a continuous background. A more general expression for the noise figure, including imperfect phase-matching, can be found in [3] and we have experimentally shown [14] that amplification for higher spatial frequencies is maximum for $\varphi \neq 0$. For a sufficiently intense input signal ($N_{\mathrm{in}} = 50$ photons), Figure 6b

$$\mathrm{NF(PSA)} = \frac{N_{\mathrm{in}}\left[N_{\mathrm{in}}\left(\cos^2(\varphi)\exp(4r) + \sin^2(\varphi)\exp(-4r)\right) + 2\cosh^2(r)\sinh^2(r)\right]}{\left[N_{\mathrm{in}}\left(\cos^2(\varphi)\exp(2r) + \sin^2(\varphi)\exp(-2r)\right) + \sinh^2(r)\right]^2} \tag{2}$$

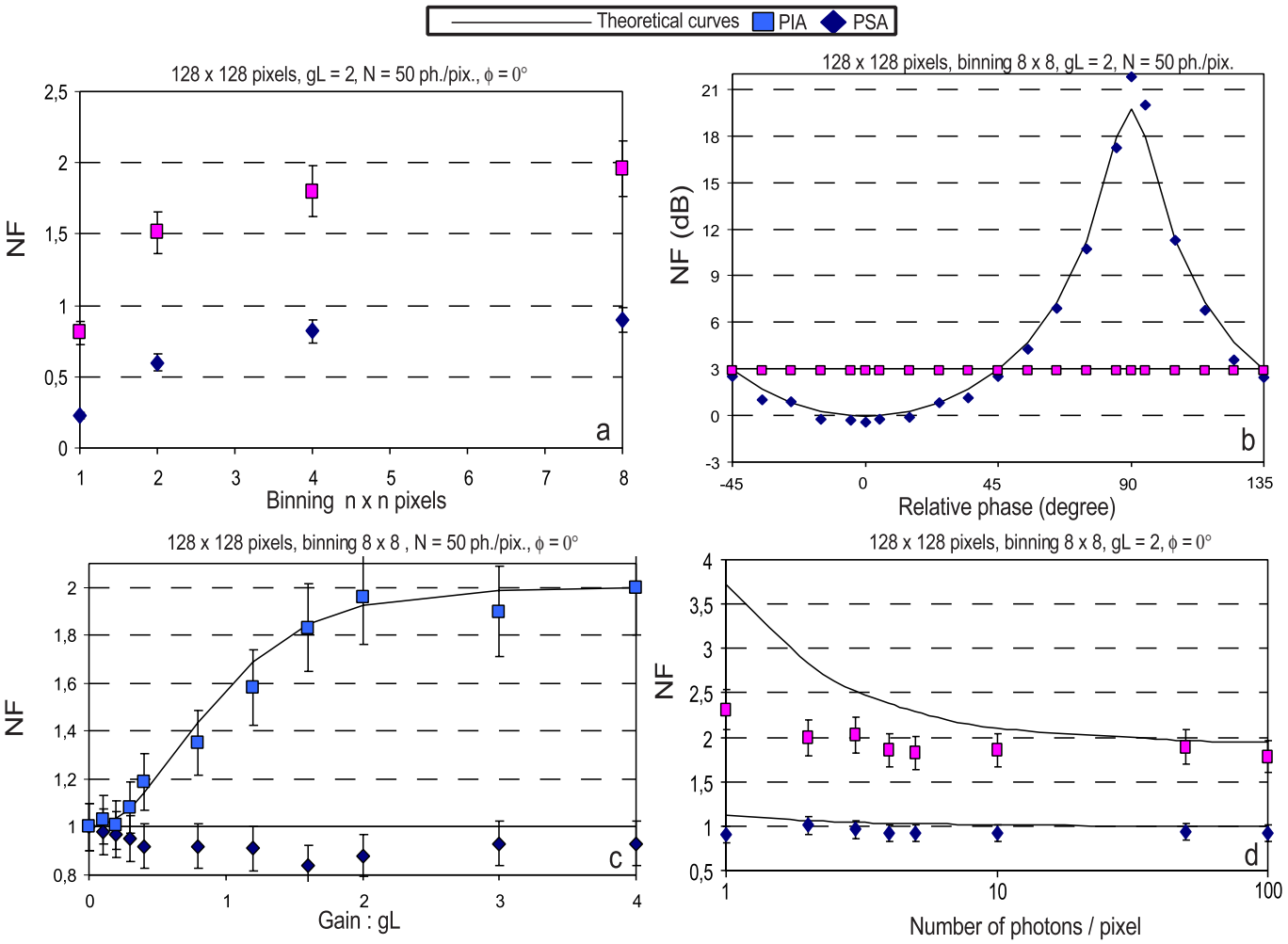

Fig. 6. Variation of the noise figure *versus*: (a) the binning, (b) the input relative phase, (c) the gain and (d) the number of photons per pixel at the input for a PSA (black curves) and a PIA (gray curves). In (b-d), the numerical simulations are fitted with the theoretical curves given by equations (4) and (5).

shows that the NF(PIA) is close to 3 dB and does not depend on the relative phase while the NF(PSA) remains close to 0 dB for a relative phase corresponding to maximum amplification. On the other hand, parametric fluorescence becomes predominant when the signal is deamplified and the noise figure attains 18 dB for maximum deamplification, in good agreement with equation (2). Note however that the output SNR becomes insignificant when fluorescence predominates. Figure 6c shows the variation of the NF with respect to the amplification gain. When the signal is injected with the phase corresponding to the amplified quadrature, NF(PSA) is equal to one whatever the gain while NF(PIA) tends to 2 when the amplification gain increases. Figure 6d shows the NF *versus* $N_{\rm in}$. When $N_{\rm in}$ decreases, NF{PSA} should become greater than 1 because the parametric fluorescence degrades the output SNR. Actually, formula (2) is questionable when $N_{\rm in}$ becomes weak because a non negligible part of the mean in the output intensity is created by the parametric fluorescence and does not carry a signal. Hence the formula (1) must be replaced at the output by:

$$\mathrm{SNR}_{\rm out} = \frac{\left(\langle N\rangle - \langle N_{\rm fluo}\rangle\right)^2}{\langle N - \langle N\rangle\rangle^2} \tag{3}$$

leading for the noise figure to:

see equation (4) below

$$\mathrm{NF(PSA)} = \frac{N_{\rm in}\left[N_{\rm in}\left(\cos^2(\varphi)\,\exp(4r) + \sin^2(\varphi)\,\exp(-4r)\right) + 2\cosh^2(r)\sinh^2(r)\right]}{\left[N_{\rm in}\left(\cos^2(\varphi)\,\exp(2r) + \sin^2(\varphi)\,\exp(-2r)\right)\right]^2} \tag{4}$$

$$\mathrm{NF(PIA)} = \frac{N_{\mathrm{in}}\left[N_{\mathrm{in}}\cosh^2(r)\left(\cosh^2(r)+\sinh^2(r)\right)+2\cosh^2(r)\sinh^2(r)\right]}{\left[N_{\mathrm{in}}\cosh^2(r)\right]^2}\,. \tag{5}$$

an equivalent expression can be derived in the phase-insensitive case:

see equation (5) above.

Figure 6d shows the numerical noise figures *versus* the number of photons, calculated with subtraction of the mean parametric fluorescence, and the theoretical curves resulting from the expressions (4) and (5). The agreement is correct except for a very low number of photons. In this case, the theoretical SNR becomes much smaller than 1 at the output, while such a very low SNR cannot be correctly estimated from the output simulated images (because the estimated signal level has no more signification).

5 Conclusion

In this paper, we have simulated the spatial fluctuations of parametric fluorescence and of the amplified image of a continuous background. The statistical analysis of these images has allowed us to define criteria that we plan to use in the next future to experimentally demonstrate noiseless image amplification, where the quantum noise is measured through purely spatial fluctuations. The simulation can be extended to other types of images, in order to assess the effect of the quantum noise on resolution. In its present form, the simulation is valid only for relatively high parametric gains, where the input quantum noise injected in a classical way has a negligible energy with respect to the output energy.

We would like to thank C. Fabre, M. Kolobov and L. Lugiato for fruitful exchanges that helped us to improve this paper. This work has been supported in part by the European Union (QUANTIM contract IST-2000-26019).

References

1. Sang-Kyung Choi, M. Vasilyev, P. Kumar, Rev. Lett. **83**, 1938 (1999).
2. M.I. Kolobov, L.A. Lugiato, Phys. Rev. A **52**, 4930 (1995).
3. I. Sokolov, M. Kolobov, L.A. Lugiato, Phys. Rev. A **60**, 2420 (1999).
4. A. Gatti, E. Brambilla, L.A. Lugiato, M.I. Kolobov, Phys. Rev. Lett. **83**, 1763 (1999).
5. T.B. Pittman, D.V. Strekalov, D.N. Klyshko, M.H. Rubin, A.V. Sergienko, Y.H. Shih, Phys. Rev. A **53**, 2804 (1996).
6. M.I. Kolobov, Rev. Mod. Phys. **71**, 1539 (1999); M.I. Kolobov, I.V. Sokolov, Sov. Phys. JETP **69**, 1097 (1989).
7. M.I. Kolobov, I.V. Sokolov, Europhys. Lett. **15**, 271 (1991); A. Gatti, L.A. Lugiato, G.-L. Oppo, R. Martin, P. Di Trapani, A. Berszanskis, Opt. Exp. **1**, 21 (1997); A. Gatti, H. Wiedemann, L.A. Lugiato, I. Marzoli, G.-L. Oppo, S.M. Barnett, Phys. Rev. A **56**, 877 (1997); I. Marzoli, A. Gatti, L.A. Lugiato, Phys. Rev. Lett. **78**, 2029 (1997).
8. C. Fabre, J.B. Fouet, A. Maître, Opt. lett. **25**, 76 (2000).
9. F. Devaux, E. Lantz, Eur. Phys. J. D **8**, 117 (2000).
10. See also the related experimental work: B.M. Jost, A.V. Sergienko, A.F. Abouraddy, B.E.A. Saleh, M.C. Teich, Opt. Expr. **3**, 81 (1998).
11. C.M. Caves, Phys. Rev. D **26**, 1817 (1982).
12. A. Levenson, I. Abram, T. Rivera, P. Grangier, J. Opt. Soc. Am. B **10**, 2233 (1993).
13. F. Devaux, E. Lantz, Opt. Commun. **114**, 295 (1995).
14. F. Devaux, E. Lantz, Phys. Rev. Lett. **84**, 2308 (2000).